



# Synthesis, characterization and evaluations of TiO<sub>2</sub> nanostructures prepared from different titania precursors for photocatalytic degradation of 4-chlorophenol in aqueous solution

Amir Payan<sup>1</sup> · Moslem Fattahi<sup>1</sup> · Behrooz Roozbehani<sup>1</sup>

Received: 19 April 2017 / Accepted: 10 January 2018 / Published online: 13 April 2018  
© Springer International Publishing AG 2018

## Abstract

**Background** The aim of present work, was to synthesize the titanium nanoparticles (TNPs) and titanium nanotubes (TNTs) through the hydrothermal method with different precursors including the Titanium(IV) isopropoxide (TTIP) and Titanium(IV) bis(ammonium lactato)dihydroxide (TALH).

**Methods** TiO<sub>2</sub> nanostructures from different titania precursors as heterogeneous photocatalysis via hydrothermal method were synthesized. The as-prepared photocatalysts were characterized by X-ray diffraction, UV–Vis diffuse reflectance spectra, surface area measurements, Fourier transform infrared spectroscopy and field emission scanning electron microscopy. The TiO<sub>2</sub> photocatalysts were tested on the degradation of 4-Chlorophenol (4-CP) aqueous solution under UVC irradiation in a fabricated photoreactor.

**Results** The effect of operating parameters including the; initial 4-CP concentration (50–150 mg/L), catalyst dosages (0–3 g/L) and solution pH (4–10) on the photocatalytic activity of the prepared catalysts were systematically investigated. The results show that amongst the TiO<sub>2</sub> nanostructures under best conditions (initial 4-CP concentration of 50 mg/L, catalyst dosage of 2 g/L, pH of 4.0, Time of 180 min) TNT-P2 exhibited much higher photocatalytic degradation efficiency (82%) as compared with TNT-P1 (77%), TNP-P2 (51%), and TNP-P1 (48%). Moreover, the mechanism and tentative pathways of 4-CP degradation were explored. Finally, the kinetic study was performed and the Langmuir-Hinshelwood kinetic model was aptly fitted with the experimental data.

**Conclusion** The results of the photocatalytic activity measurement demonstrated that one-dimensional TNTs shows enhanced photocatalytic performance as compared to the TNPs, therefore, indicating the beneficial feature of TNTs as a photocatalyst for the degradation of pollutants. Besides, TiO<sub>2</sub> nanostructures prepared from TALH precursor (TNT-P2 82%, TNP-P2 51%) has higher photocatalytic degradation efficiency as compared with TTIP precursors (TNT-P1 77%, TNP-P1 48%).

**Keywords** Titanium nanostructures · Photocatalytic · UV irradiation · Hydrothermal method

## Background

In the past three decades, chlorinated organic compounds (COCs), which are classified as primary contaminants, have

been extensively used in various industries [1]. Chlorophenols (CPs) come under the sub-category of COCs as the main groups of ecotoxins and these enter the environment as a result of the use of chlorination for disinfectant purposes or as an industrial byproduct. CPs, which are recognized as very low biodegradable organic materials, are categorized in the class of organohalogen priority toxic chemicals listed as hazardous substances when discharged into surface waters (vide the EU council directive 2006/11/EC) [2]. In addition, the U.S. Environmental Protection Agency (US EPA) has announced that chlorophenols are priority pollutants [3].

The presence of 4-CP in the wastewater of oil refineries, the petrochemical industry, and dye synthesizing endangers human health and aquatic life [4, 5]. Conventional treatment techniques used to eliminate this compound include

✉ Moslem Fattahi  
fattahi@put.ac.ir

Amir Payan  
ahp8329@gmail.com

Behrooz Roozbehani  
roozbehani@put.ac.ir

<sup>1</sup> Department of Chemical Engineering, Abadan Faculty of Petroleum Engineering, Petroleum University of Technology, Abadan, Iran

adsorption and biological treatment; however, a long treatment time is required [6]. Therefore, an effective conversion of 4-CP to harmless material is highly desirable with regard to water decontamination [7].

Advanced oxidation processes (AOPs), including Fenton, catalytic wet air oxidation and heterogeneous photocatalysis are known as favorable alternatives to the traditional treatment techniques, as they open greener pathways for the complete mineralization of environmental contamination and have been effectively used for the purification of polluted water and soil [8, 9].

Wang et al. used  $\text{Fe}_2\text{O}_3$  nanoparticles with different hydroxyl content for 4-CP oxidation in one partial solution and in a mixed solution of Cr(VI) + 4-CP. The  $\text{Fe}_2\text{O}_3$  photocatalyst exhibited 13.5 and 47.8% 4-CP oxidation, respectively [10]. Wang et al. utilized a heterogeneous Fenton-like photocatalyst to adsorb and remove 4-CP in aqueous solution and reported a completed removal in presence of  $\text{H}_2\text{O}_2 + \text{Fe}_3\text{O}_4 + \beta\text{-CD}$  at 90 min [11]. To study the photocatalytic activity of  $\text{TiO}_2$  in visible and solar light for 4-CP degradation some researches were performed by doping metals and nonmetals such as Zn, Co, Cu, Ni, Ag, Pd, La, N, C, P [3, 12–14]. Moreover, Pozan and Kambur described a high improvement in photocatalytic activity by means of the bifunctional ZnO- $\text{TiO}_2$  photocatalyst. The 4-CP conversion at 75 min, at natural pH, follows the order as: 20 wt% ZnO (100%) > 50 wt% ZnO (87%) > 80 wt% ZnO (78%) [15]. Zouzelka et al. reported a procedure for fabrication of adherent nanoparticle mesoporous layer. They investigated the effect of pure anatase, Brookite and P25 films as well as nanocomposite coatings mixing MWCNT and anatase in the degradation of aqueous solutions of 4-CP [16]. Zhai et al. synthesized an iron-containing silicotungstate ( $\text{Fe}^{\text{III}}\text{LysSiW}$ ) and applied for 4-CP oxidation as the heterogeneous Fenton-like catalyst. The prepared  $\text{Fe}^{\text{III}}\text{LysSiW}$  exhibited high photocatalytic efficiency for 4-CP removal at pH of 7 under both the irradiated and dark conditions so that under the conditions of  $\text{Fe}^{\text{III}}\text{LysSiW}$  1.0 g/L,  $\text{H}_2\text{O}_2$  20 mmol/L and 4-CP 100 mg/L, the TOC elimination attained to 98.8% under irradiation and 71.3% in the dark [17]. Naem et al. examined the effect of supports on the photocatalytic performance of  $\text{TiO}_2$  nanoparticles. Among the three supports, namely activated carbon (AC), silica ( $\text{SiO}_2$ ) and zeolite (ZSM-5), all showed high performance for degradation of 4-CP and were better than bare  $\text{TiO}_2$ . The efficiency order of these three supports was as follows: AC > ZSM-5 >  $\text{SiO}_2$ , respectively [18]. Di et al. improved photocatalytic activity of homogeneous carbon superdoped  $\text{BiPO}_4$  via the ionic liquid (IL) [Omim]  $\text{H}_2\text{PO}_4$  induced process. The C- $\text{BiPO}_4$  displayed an increase in photocatalytic activity for the degradation of 4-CP under the UV light irradiation [19].

The synthesis of the  $\text{TiO}_2$ -based nanostructures during hydrothermal treatment is impacted by various parameters and conditions including the Ti precursors type, pre-hydrothermal

treatments, time and temperature of hydrothermal synthesis, and post-hydrothermal treatments (washing and calcination process) [20, 21]. It has been reported that the different starting Ti materials can affect the morphology and characteristics of the  $\text{TiO}_2$ -based nanostructures such as the crystal structure, thermal stability, specific surface area and consequently influence the photocatalytic activity performance of the prepared nanostructures [21–23]; therefore the Ti precursor type is a key factor in  $\text{TiO}_2$ -based nanostructures fabrication and application.

On the other hand, there is an extensive availability of Ti precursor groups that were employed in fabrication of  $\text{TiO}_2$ -based nanostructures including the; titanium alkoxides (i.e., titanium isopropoxide, titanium butoxide, titanium ethoxide), titanium halides (i.e.,  $\text{TiCl}_4$  and  $\text{TiF}_4$ ), titanatranes, titanium(IV) bis(ammonium lactato) dihydroxide and titanium sulfate and oxysulfate ( $\text{Ti}(\text{SO}_4)_2$  and  $\text{TiOSO}_4$ ) [24]. Thus, with considering these factors, choosing the right Ti precursor for high performance fabrication and application of the  $\text{TiO}_2$ -based nanostructures seems to be very necessary. There are only a few studies that investigated the effect of Ti precursors in the photocatalytic activities [25–27]. The main drawback associated with this limited studies is that all of these works explored the titania precursors which belong to one Ti precursor group (mainly titanium alkoxides group). To the best of our knowledge, there is no investigation that has compared and examined the photocatalytic activity performance of the  $\text{TiO}_2$ -based nanostructures that were prepared from two different titania precursor groups. For this aim, in the present work, two different types of titanium precursor were investigated including the Titanium(IV) isopropoxide from alkoxides group and Titanium (IV) bis(ammonium lactato) dihydroxide. In two-step procedure, from each precursor, titanium nanoparticles (TNPs) and titanium nanotubes (TNTs) through hydrothermal method were synthesized. The synthesized nanostructures from morphological, optical and structural properties point of view were characterized. Then, the photocatalytic activity of nanostructures was examined for degradation of 4-CP under UVC irradiation. Furthermore, the effects of operating parameters on 4-CP degradation were studied.

## Methods

### Materials

Titanium(IV) isopropoxide (TTIP 99.9%) and Titanium(IV) bis(ammonium lactato)dihydroxide (TALH 50%) from Sigma-Aldrich (USA) were purchased and utilized as the precursors of catalysts. Chemicals including sodium hydroxide,

nitric acid 65%, hydrochloric acid 37%, methanol, and urea were purchased from Merck Company, Germany. 4-CP was purchased from Sigma-Aldrich, USA. All materials were analytical grade and used without further purifications.

### Synthesis of catalysts

Two types of titanium precursors were used in the present study. First of these, titanium isopropoxide (TTIP; 8.8 mL), was dropwise added to a 300 mL water and ethanol solution (at a 4:1 ratio) in a typical synthesis. Nitric acid was added to obtain a transparent solution and the solution pH was approximately 7 at this time. This transparent solution was stirred for 2 h, after which it was placed in an autoclave and hydrothermally crystallized at 250 °C for 5 h. After cooling, the precipitate washed with distilled water and separated by centrifugation, then the samples dried in a vacuum oven at 85 °C for 18 h. Finally, it underwent a calcination process at 400 °C for 6 h [28].

In the next step, for synthesizing titanium nanotubes (TNT-P1), titanium nanoparticles, as obtained from the first precursor, denoted TNP-P1 (0.5 g), were mixed with 40 mL of aqueous solution 10 M NaOH, placed in an autoclave and hydrothermally crystallized at 150 °C for 13 h. After cooling, the precipitate was separated by centrifugation and washed with distilled water and HCl of 0.1 M until a precipitate with a pH of approximately 8 was obtained. This precipitate was then dispersed in absolute ethanol by ultrasonic dispersion for 30 min [29]. After a second centrifugation, the sample was dried and calcinated in the same way as described above.

As a second precursor, titanium(IV) bis(ammonium lactato) dihydroxide (TALH; 10 mL) was thermally hydrolyzed in the presence of 90 mL of 0.1 M urea at 170 °C for 20 h [30]. The precipitate was then centrifuged, washed, dried and calcinated in a similar manner to that described above and result denoted TNP-2. Titanium nanotubes from the second precursor, denoted TNT-P2, were prepared in the same way as TNT-P1, that described above.

### Characterization

X-ray diffraction (XRD) of the specimens was conducted using a X-ray diffractometer (Philips, PW1730, Netherland), with Cu  $K_{\alpha}$  radiation ( $\lambda = 0.15406$  nm) in the range of  $2\theta = 5^{\circ}$ – $80^{\circ}$ , with a step size of  $0.05^{\circ}$  for confirming and analyzing the phase structure. Ultraviolet (UV)-vis diffuse reflectance spectra were acquired using a UV-vis spectrometer (Avantes, AvaSpec-2048-TEC, Netherland) along with a 150 mm integrating sphere. Fourier transform infrared (FTIR) spectroscopic analysis of the prepared materials was performed on a FTIR

instrument (Bruker, VERTEX70, Germany). The specific surface areas of the samples were measured by  $N_2$  adsorption-desorption isotherms at 77 K, using a adsorption apparatus (Bel, Belsorp-mini II, Japan) based on Brunauer-Emmett-Teller theory. Mean pore diameter and pore volume were determined by the  $N_2$  adsorption volume at a relative pressure of 0.99, using a Barrett-Joyner-Halenda (BJH) technique. The morphology of the materials was analyzed by a MIRA3 field emission scanning electron microscope (TESCAN, Mira 3, Czech Republic) operating at 15.0 kV. The dispersion of the samples was performed using Ultrasonic homogenizer apparatus (FAPAN, 400UT, Iran). The intermediates and by-products reactions were evaluated using the Agilent 6100 Series Quadrupole LC/MS system.

### Photocatalytic activity test

The activities of the  $TiO_2$  nanostructure photocatalysts were investigated via degradation of 4-CP as a target pollutant, in a locally fabricated photocatalytic reactor. The reactor consisted of a rectangular glass cell with a 480 mL volume (30 mm  $\times$  4 mm  $\times$  4 mm), with magnetic stirring (Heidolph, MR3001 K, Germany). Figure 1 shows a schematic diagram of photo-reactor. Two UVC lamps, with a wavelength centered at 254 nm (Philips, TUV 8 W/G5 T5, Netherland), were used as the light source and a

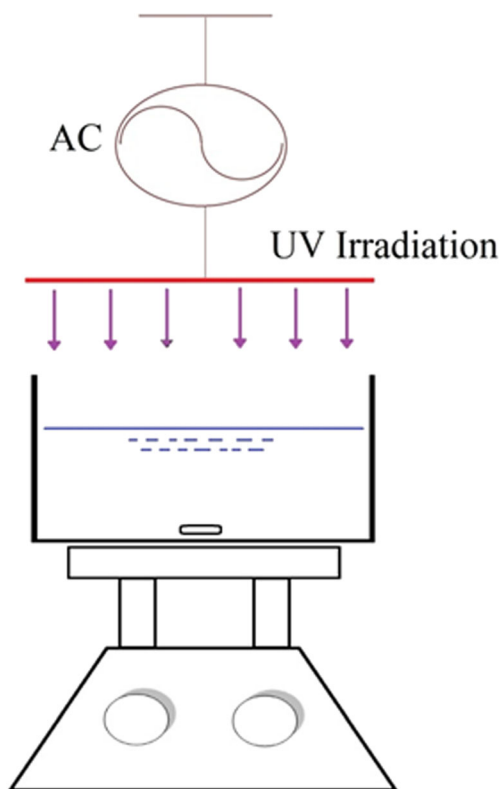
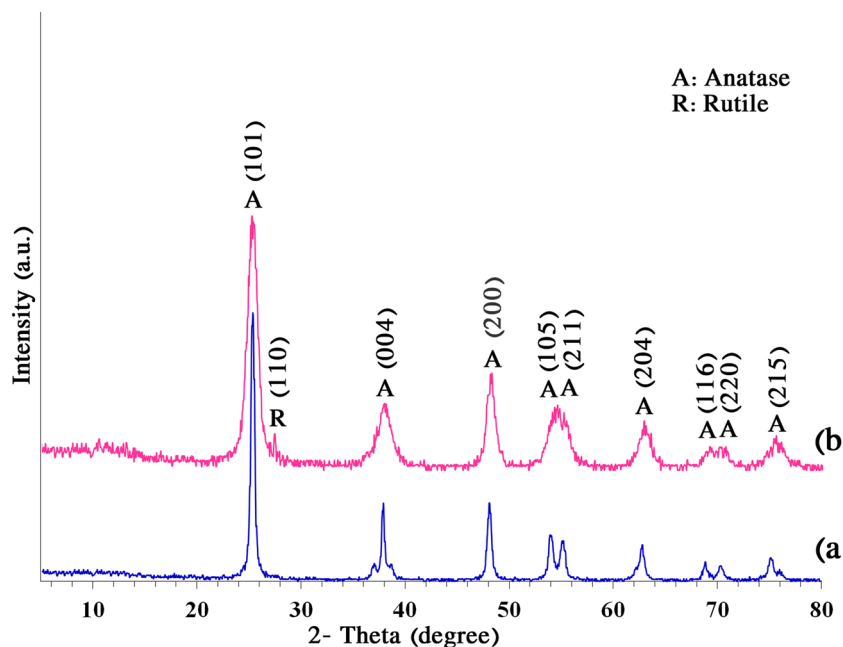


Fig. 1 Schematic of photoreactor for 4-CP degradation

**Fig. 2** XRD patterns of the **a** TNP-P1 and **b** TNP-P2



metallic cover was placed outside to isolate other light sources. Various amounts of catalyst were added to the 240 mL aqueous solution containing 4-CP. The mixture was stirred for 30 min without irradiation to identify the adsorption and desorption that was required for equilibrium.

The solution pH was controlled by adding 0.1 N HCl or NaOH and monitoring with a digital pH meter (Jenway, 3510, United Kingdom) and the temperature of the reactor was maintained at  $25 \pm 1$  °C with an air conditioning system. During the experiments, 5 mL of suspension was periodically

withdrawn from the photoreactor. The photocatalysts were separated by centrifugation (Universal, PIT320, Iran) and the resulting transparent solution was investigated using UV spectroscopy (Unico, UV2100, USA). Finally, 4-CP degradation was measured through the following equation [31]:

$$\% \text{Degradation} = \left[ \frac{C_0 - C}{C_0} \right] \times 100 \quad (1)$$

where  $C_0$  is the initial concentration of 4-CP and  $C$  is the concentration of 4-CP at any time.

**Fig. 3** XRD patterns of the **a** TNT-P1 and **b** TNT-P2

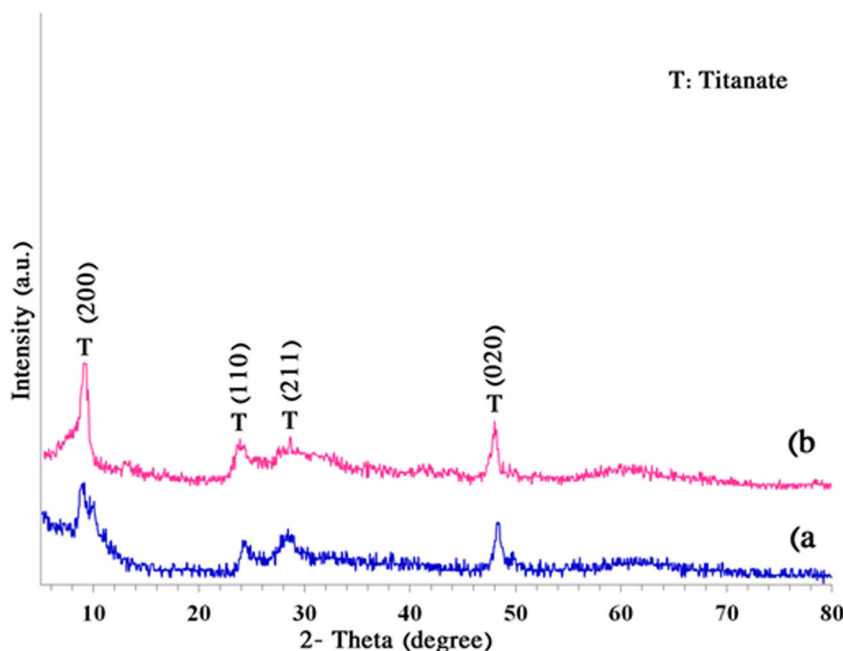


**Table 1** Average size and anatase or rutile composition of the TNP-P1 and TNP-P2

Catalyst	Anatase (%)	Rutile (%)	Size (nm)
TNP-P1	100	0	17
TNP-P2	87	13	7

**Availability of data** We agree to share our data and materials.

## Results and discussion

### XRD

Figure 2 depicts the XRD patterns of TNP-P1 and TNP-P2. The sharp peaks observed at 25.3°, 38.1°, 48.1°, 54.1°, 55.6°, 62.7°, 68.8°, 70.5° and 75.2° were indexed to (101), (004), (200), (105), (204), and (215) crystal faces of the anatase phase of TiO<sub>2</sub> (JCPDS Card No. 21–1272). The diffraction peak at 27.2° in the XRD pattern of TNP-P2 was consistent with rutile (110) spacing (JCPDS Card No. 21–1276), whereas TNP-P1 had only pure anatase peaks. The XRD patterns of TNT-P1 and TNT-P2 are illustrated in Fig. 3. The TNT phase was recognized on the basis of diffraction peaks at 9.8°, 24.2°, 28.6°, and 48.1° to Miller indices of (200), (110), (211) and (020), respectively. It was identified that the tubular framework structure of the TNT was formed, and was in accordance with previously published results [29, 32]. The average size of TiO<sub>2</sub> crystallites was estimated by Scherrer’s equation [33]:

$$D = \frac{0.9\lambda}{\beta \cos \theta} \tag{2}$$

where  $\lambda$  is the X-ray wavelength consistent to Cu K $\alpha$  radiation

(0.15406 nm),  $\beta$  is the broadening (in radians) of the anatase (101) reflection, and  $\theta$  is the angle of diffraction corresponding to the peak broadening. Moreover, to calculate the anatase level relative to rutile from the peak intensities, the Spurr-Myers equation [34] was utilized, as follows:

$$\% \text{anatase} = \frac{1}{1 + 1.26 \frac{I_R}{I_A}} \tag{3}$$

where  $I_R$  is the (110) peak intensity of rutile,  $I_A$  is the (101) peak intensity of anatase and 1.26 is the scattering constant. Table 1 represented the average size of the particles and percentage phase that were calculated through Eqs. (1) and (2), respectively.

### Diffuse reflectance spectra

The absorption spectra of different TiO<sub>2</sub> nanostructures are presented in Fig. 4. All samples shown in this figure had obvious adsorption in the UV region and adsorption in the visible light range was near to zero. The band gap calculation of all samples was carried out using Planck’s equation [35], as below:

$$E_{bg} = \frac{hc}{\lambda} \tag{4}$$

where  $h$  is the Planks constant ( $4.135667662 \times 10^{-15}$  eV),  $C$  is the speed of light ( $2.99792458 \times 10^8$  m/s) and  $\lambda$  is the cut off wavelength. As can be observed in Table 2, the band gap of TNP-P2 was greater than TNP-P1. This phenomenon is related to two factors: a) delocalization of molecular orbitals, which in turn creates energy traps and surface states on the band edge, and b) the size quantization effect [35]. When the particle size decreases, the band gap energies increase, as size quantization

**Fig. 4** DRS spectra of the synthesized nanomaterials

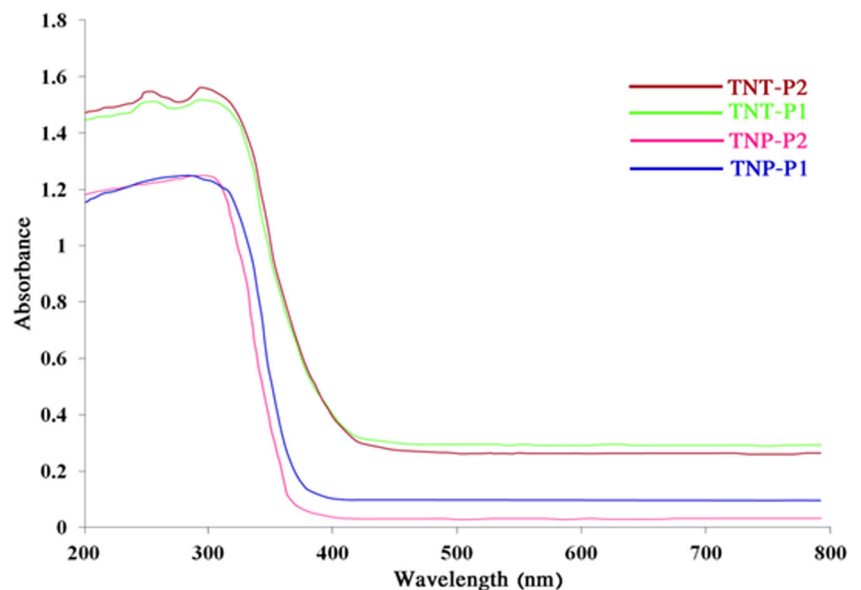




**Table 2** Surface area, total pore volume and average pore diameter of the prepared materials via the BET method

Catalyst	Surface area ( $\frac{m^2}{g}$ )	Total pore volume ( $\frac{cm^3}{g}$ )	Average pore diameter (nm)	Band gap (eV)
TNP-P1	46.242	0.346	29.992	3.17
TNP-P2	61.314	0.155	10.151	3.31
TNT-P1	138.830	0.815	23.481	2.78
TNT-P2	167.582	0.643	15.347	2.79

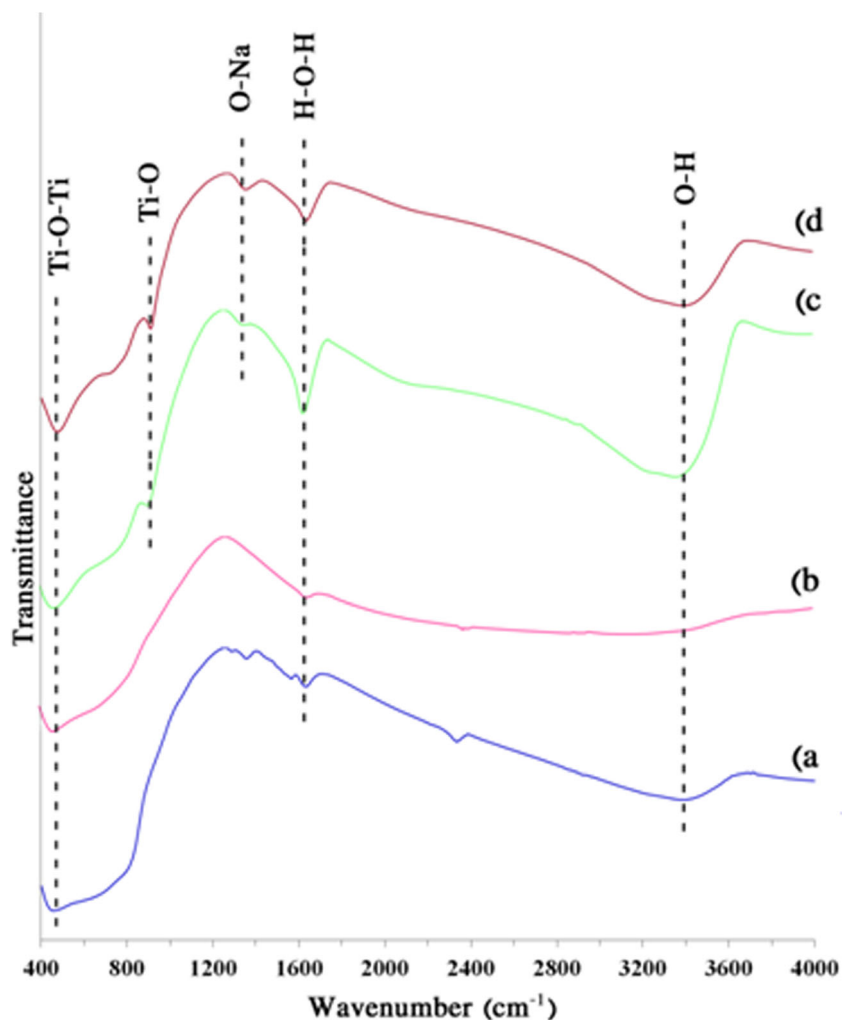
results in a shifting of the absorption edge to higher energies [36]. In general, the band gap of TNTs is smaller than TNPs, which is ascribed due to the formation of localized electronic states of oxygen vacancies in the band gap of  $TiO_2$  [37]. In comparison, the diameter of the TNTs when is larger than 1.3 nm, as in this case, the band gaps are very close in their values [38].

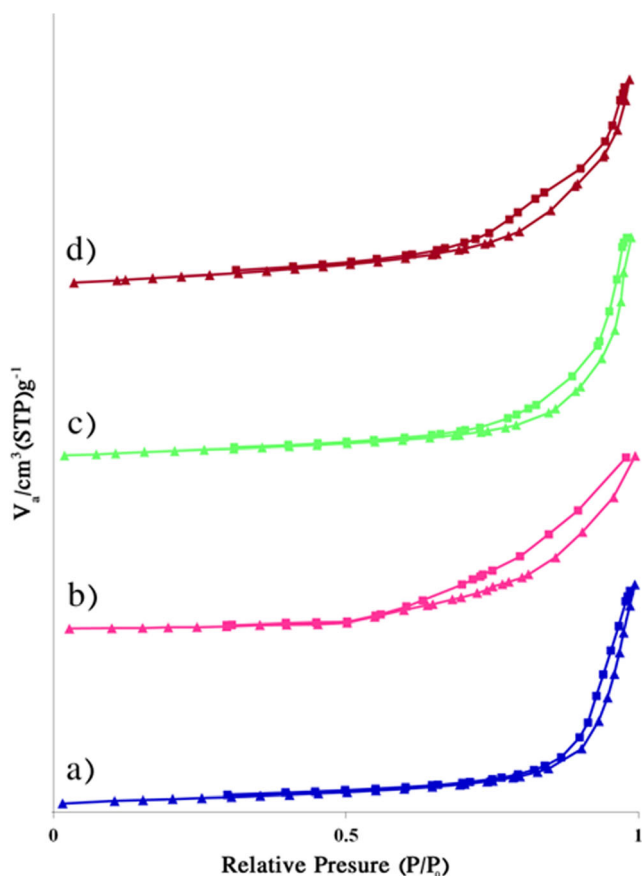
## FTIR

Figure 5 presents the FTIR spectra of the  $TiO_2$  nanostructures in the range of 400–4000  $cm^{-1}$ . The obtained results clearly

indicate that there was a stretching vibration at 460  $cm^{-1}$  with different intensity for all of the catalysts, which can be ascribed to the vibration of the  $[TiO_6]$  octahedron [39]. The peak observed at approximately 910  $cm^{-1}$  in the TNTs samples was due to four-coordinate Ti-O stretching vibration involving non-bridging oxygen atoms that were coordinated with Na ions. The TNTs also showed a peak at 1353  $cm^{-1}$  that was related to the O-Na stretching vibration [40, 41]. Strong broad peaks can be observed at 1630 and 3440  $cm^{-1}$ , attributed to the H-O-H binding vibration and the O-H stretching vibration, respectively, indicating the existence of hydroxyl groups and surface-adsorbed water molecules [42].

**Fig. 5** FTIR spectra of the **a** TNP-P1, **b** TNP-P2, **c** TNT-P1 and **d** TNT-P2





**Fig. 6** Adsorption-desorption spectra of the **a** TNP-P1, **b** TNP-P2, **c** TNT-P1 and **d** TNT-P2

**Surface analysis**

The surface area, average pore diameter and pore volume of samples were measured using the N<sub>2</sub> adsorption-desorption method. The adsorption data showed that the total pore volume and surface area of the TNPs obviously increased after hydrothermal treatment, indicating the formation of the tubular structure of TiO<sub>2</sub> (Table 2). As shown in Fig. 6, the N<sub>2</sub> adsorption-desorption isotherms for all samples fitted type III isotherms according to IUPAC nomenclature [31]. This type is attributed to macroporous materials, but hysteresis loops observed in the isotherms showed that they are typical of mesoporous materials [43]. In order to determine pore size distributions, the BJH method was employed which the results confirmed the existence of mesopores (Fig. 7). Moreover, the tubular structure of TNTs resulted in an increase of total pore volume, to ensure that both TNTs were opened and that N<sub>2</sub> gas molecules could thus access the inner pores [41]. This mesoporous catalyst is synthesized to represent a good performance in photocatalytic activities.

**FE-SEM analysis**

In order to obtain information regarding the morphology of the particles, some selected powders were investigated using

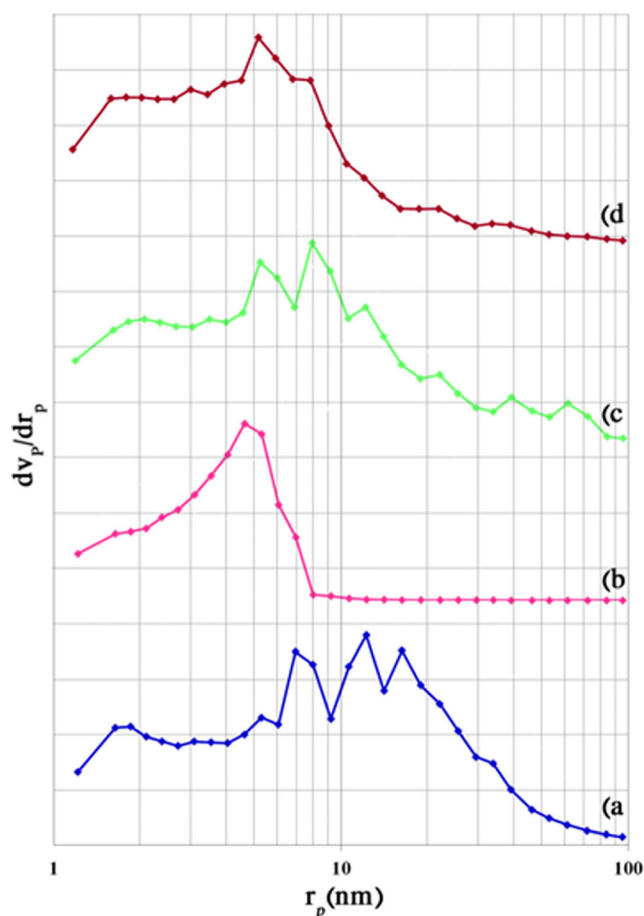


**Fig. 7** Pore size distributions of the **a** TNP-P1, **b** TNP-P2, **c** TNT-P1 and **d** TNT-P2

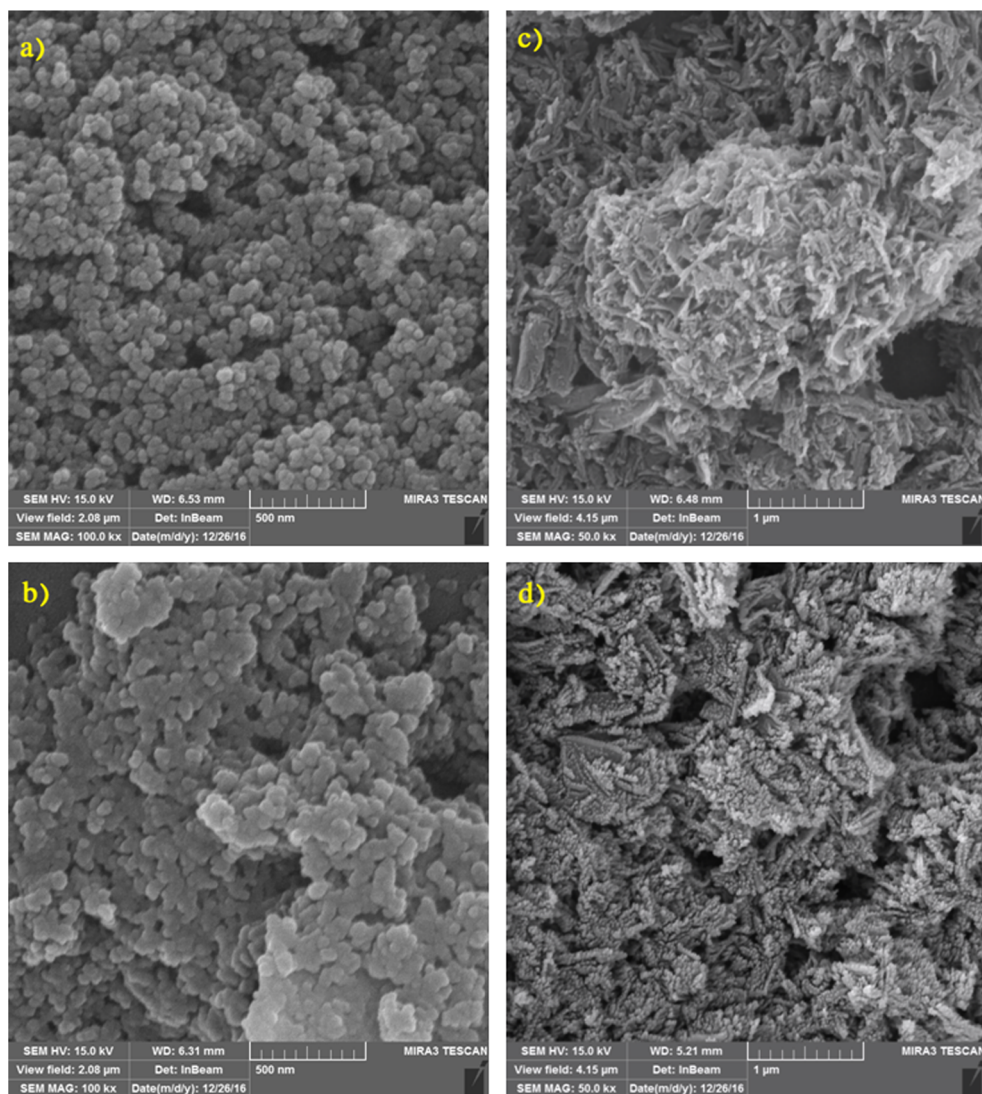
FE-SEM. As Fig. 8(a-d) shows, the TNPs samples roughly existed in a form of spherical particles and presented porous structures. The size of the TNP-P2 nanoparticles observed in the FE-SEM images was smaller than that of the TNP-P1 nanoparticles, which is in accordance with the value calculated using the XRD. As the FE-SEM image shows, the TiO<sub>2</sub> nanotubes had a tubular and uniform morphology.

**Photocatalytic degradation**

**Effects of 4-CP concentration on degradation process**

The initial concentration of a pollutant has an important role in any water treatment process, so an investigation of its influence on the performance of the process appears to be necessary. In this study, different initial concentrations of 4-CP, ranging from 50 to 150 mg/L, were examined. As shown in Fig. 9 (a-d), the degradation rate decreased with increasing 4-CP concentration, indicating the limitation in the amount of reactive species produced by the UV illumination. The generation of hydroxyl radicals was constant for specific amounts of the catalyst; therefore, the accessible hydroxyl radicals were

**Fig. 8** FE-SEM images of **a** TNP-P1, **b** TNP-P2, **c** TNT-P1 and **d** TNT-P2



not sufficient to degrade 4-CP at higher concentrations. Moreover, the higher 4-CP concentration produced the higher concentrations of intermediate products, which competed for reaction with the hydroxyl radicals [44]. It is obvious that the amounts of 4-CP removed by the catalysts increase with increasing initial concentrations; however, their photodegradation rates decrease with initial concentrations. These findings are consistent with previous studies [45–47].

#### Effects of catalyst dosages on degradation process

The effects of various dosages of  $\text{TiO}_2$  photocatalysts on the efficiency of 4-CP photocatalytic degradation were investigated. As shown in Fig. 10(a–d), the variation in the percentage degradation of 4-CP according to the concentration of  $\text{TiO}_2$  was examined using a photocatalyst dosage range of 0–3 g/L. The results showed that 4-CP photocatalytic degradation efficiency improved with increasing catalyst dosage [48]. However,

at a higher  $\text{TiO}_2$  load, a decrease in 4-CP degradation was observed. This phenomenon may be ascribed to the increase of the total active surface area of the photocatalysts available for photocatalytic reaction; they result in greater generation of hydroxyl and/or superoxide radicals when the catalyst dosage is increased. When the  $\text{TiO}_2$  load is greatly increased, the aggregation of catalyst particles at high concentration leads to a decrease in the number of surface active sites, resulting in an increase of opacity and light scattering of  $\text{TiO}_2$  nanostructures at high concentrations, leading to a decrease in the passage of irradiation over the samples [49].

#### Effects of pH on degradation process

The solution pH has a strong influence on the degradation of pollutants in the aqueous phase. The pH effects photocatalyst surface charge, physiochemical properties, adsorption and dissociation of the substrate and the oxidation potential of the



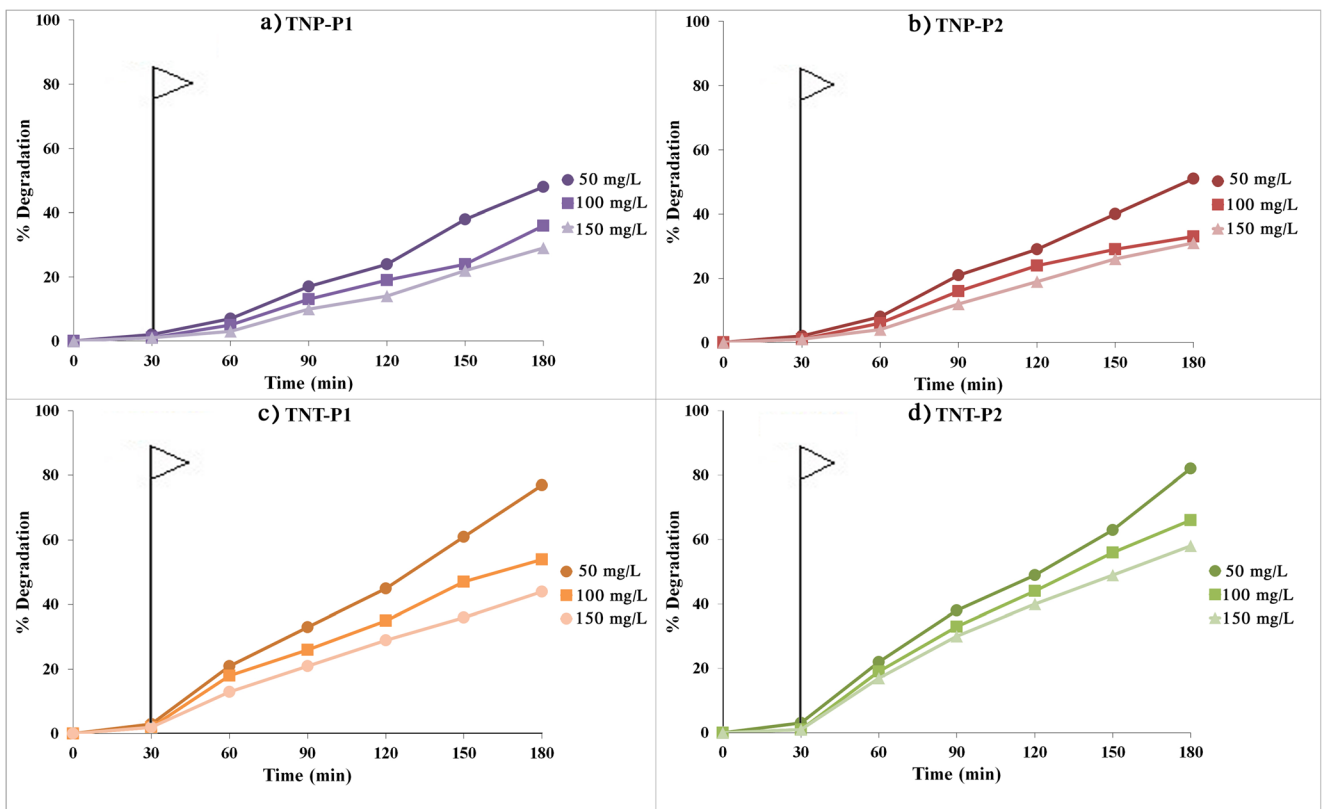


Fig. 9 Effect of different initial 4-CP concentration on degradation process for a TNP-P1, b TNP-P2, c TNT-P1 and d TNT-P2

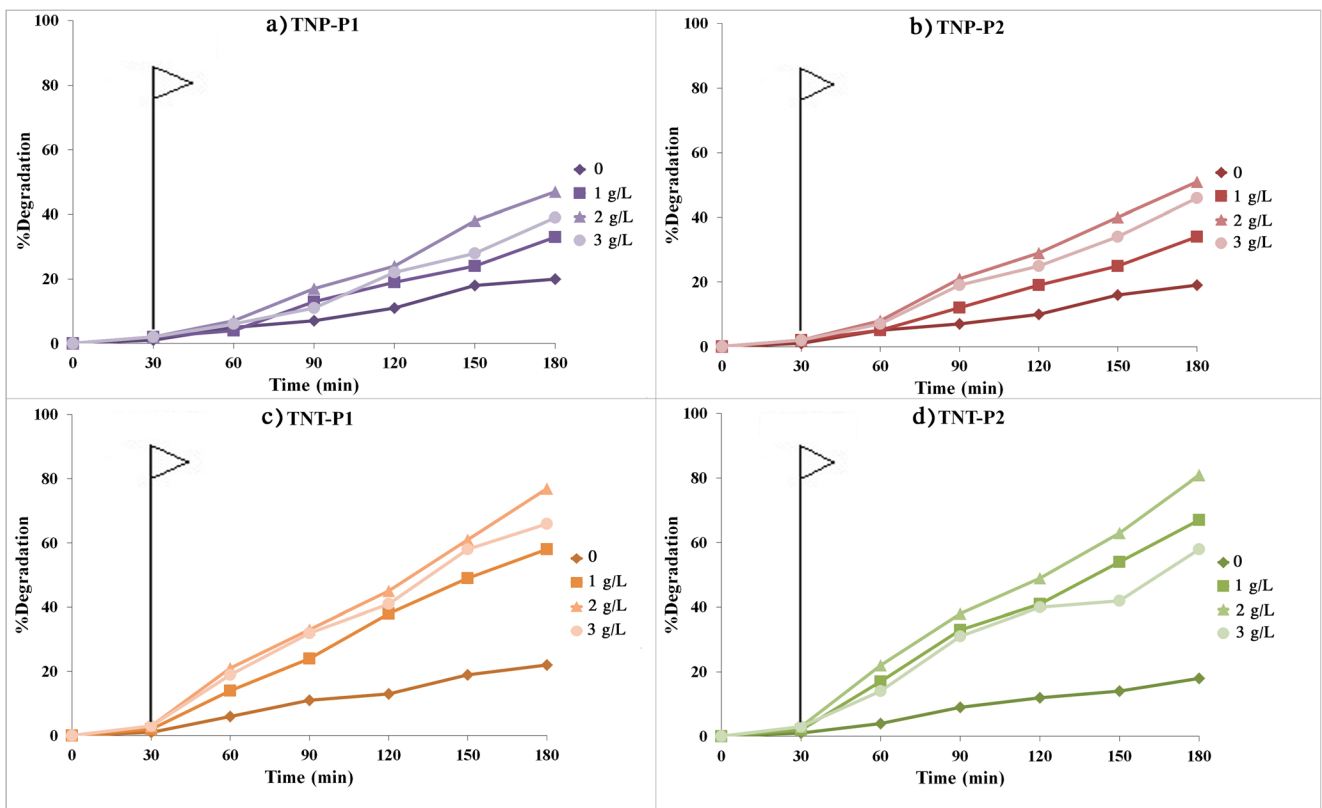
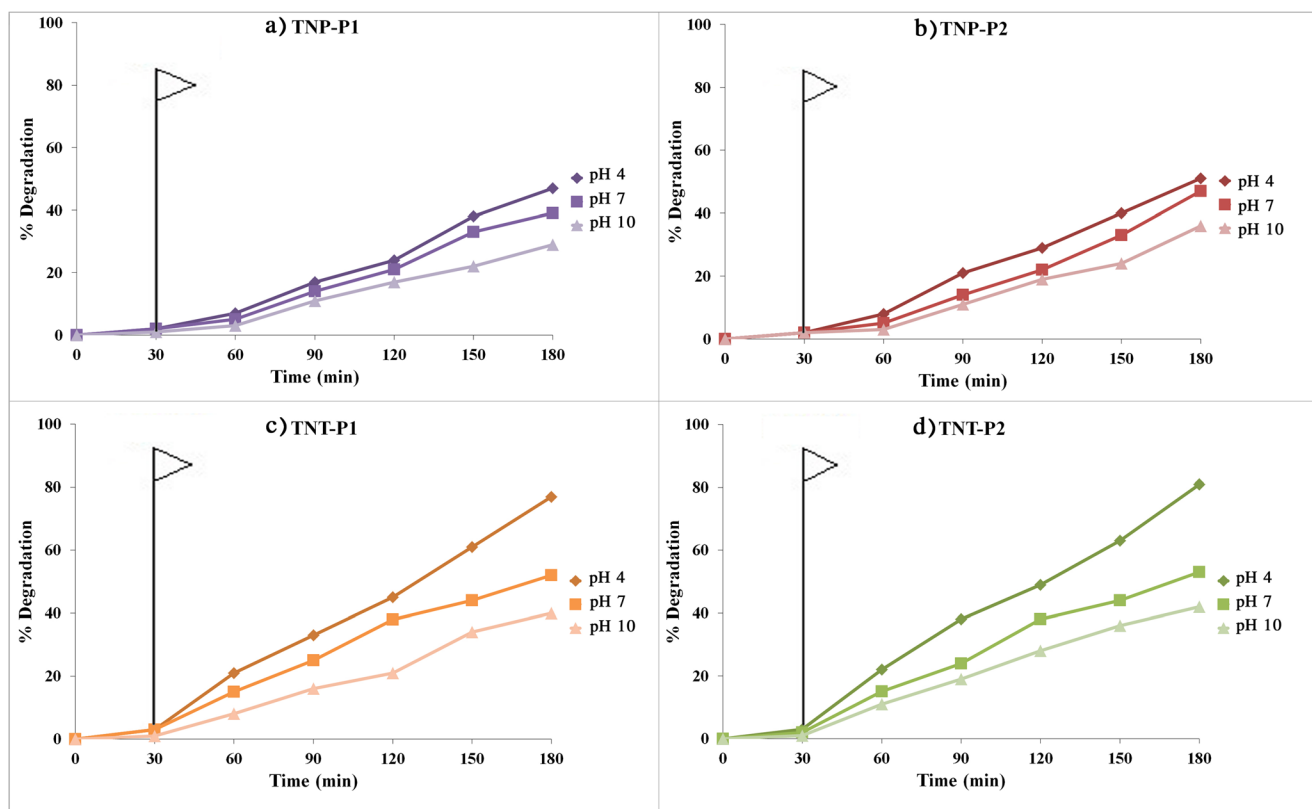


Fig. 10 Effect of different  $TiO_2$  dosages on degradation process for a TNP-P1, b TNP-P2, c TNT-P1 and d TNT-P2

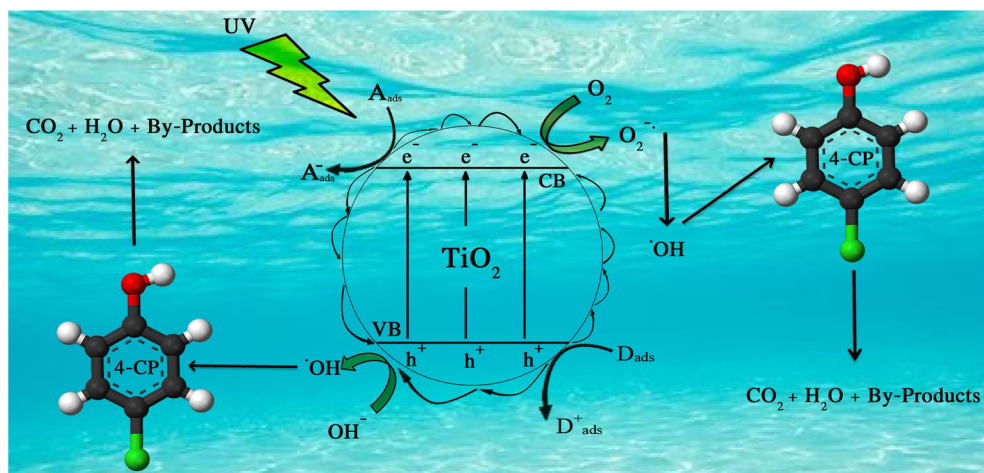


**Fig. 11** Effect of initial pH solution on degradation process for **a** TNP-P1, **b** TNP-P2, **c** TNT-P1 and **d** TNT-P2

valence band (VB) [44]. The role of initial pH levels on photocatalytic degradation of 4-CP was examined by varying the pH values from 4 to 10. As shown in Fig. 11(a–d), the rates of degradation decreased with increasing pH. The charge at the surface is associated with both the initial solution pH and the zero point charge of the  $\text{TiO}_2$ . If the solution pH is greater than the zero point charge, the surface is charged negatively; thus, at lower pH, the surface is charged positively [50]. Previous studies have shown that the zero point charge ( $\text{pH}_{\text{zpc}}$ ) of  $\text{TiO}_2$  is 6.9 [51]. Therefore, decreasing the solution pH slowly

changes the surface charge of  $\text{TiO}_2$  from negative to positive; in addition, 4-CP changes to the phenolate anion form above a pH of 10. The decrease of 4-CP photocatalytic degradation in alkaline medium is related to the electrostatic repulsion between the negatively charged  $\text{TiO}_2$  surface and the 4-CP anion that is hindering the 4-CP/ $\text{TiO}_2$  interaction [52]. In addition, the rate of 4-CP degradation at low initial pH value is high, because the more  $\text{H}^+$  ions are in the solution, the more conduction band electrons ( $e^-$ ) can transfer to the surface of the catalyst to react with  $\text{O}_2$  to generate more hydroxyl radicals

**Fig. 12** The tentative mechanisms for the photocatalytic degradation of 4-CP using the  $\text{TiO}_2$  nanostructures under UV irradiation in aqueous solution



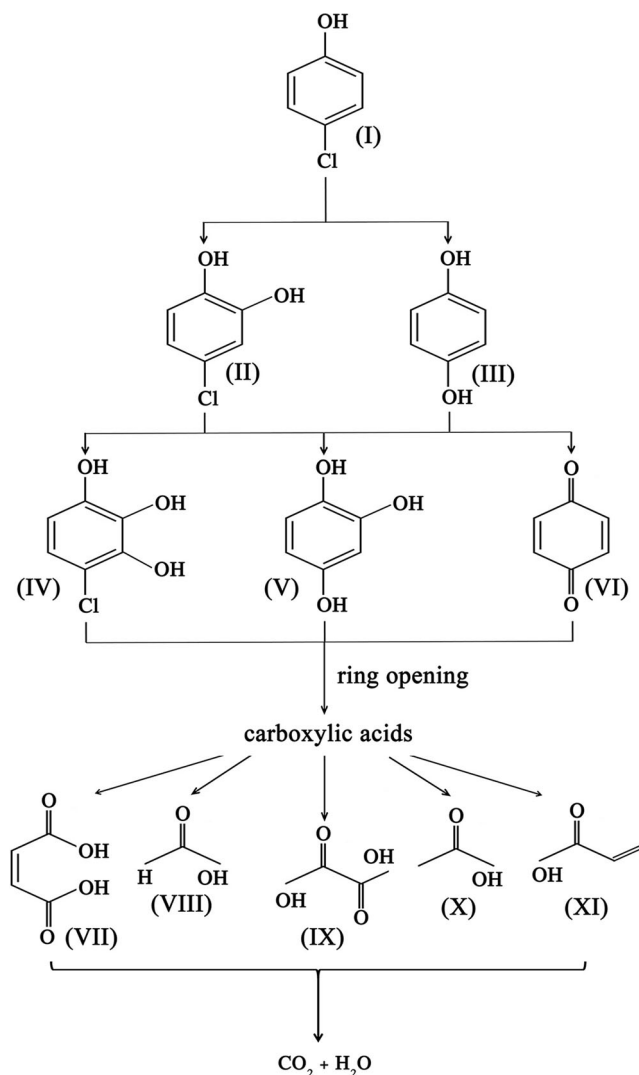


Fig. 13 Proposed reaction pathway for degradation of 4-CP

[53]. Moreover, reduction of the electron-hole recombination in the acidic medium is another significant factor for improving of 4-CP degradation [54].

**Photocatalytic degradation mechanism and pathway**

The process of 4-CP photocatalytic degradation is started with the absorption of an impressive number of photons by photocatalyst and photo-induced electrons and holes formed on the photocatalyst surface as illustrated in Fig. 12. The electrons relocated from the VB to the conduction band (CB) of TiO<sub>2</sub>; at the same time, the positive holes (h<sup>+</sup>) are produced in the VB. On one hand, the excited state electrons can be trapped by the dissolved O<sub>2</sub> which adsorbed on the catalyst surface and formed the O<sub>2</sub><sup>•-</sup> radicals. Then O<sub>2</sub><sup>•-</sup> react with adsorbed H<sub>2</sub>O to produce H<sub>2</sub>O<sub>2</sub> which generate hydroxyl radicals (OH) [55]. On the other hand, the photo-induced holes in VB can react with OH<sup>-</sup> to generate more OH<sup>•</sup> radicals [56].

These series of reaction are listed as follows:

$$TiO_2 + hv \rightarrow h_{VB}^+ + e_{CB}^- \tag{5}$$

$$O_2 + e_{CB}^- \rightarrow O_2^{\bullet -} \tag{6}$$

$$2O_2^{\bullet -} + 2H_2O \rightarrow H_2O_2 + 2OH^- + O_2 \tag{7}$$

$$H_2O_2 + e_{CB}^- \rightarrow OH^- + OH^{\bullet} \tag{8}$$

$$h_{VB}^+ + OH^- \rightarrow OH^{\bullet} \tag{9}$$

After generation of O<sub>2</sub><sup>•-</sup> and OH<sup>•</sup> as the most important oxidative radicals, these radicals attack the 4-CP molecule. A proposed degradation pathway of 4-CP by TiO<sub>2</sub> photocatalyst was illustrated in Fig. 13. During the 4-CP oxidation, a number of aromatic intermediates are formed that first five main intermediates are hydroquinone (HQ, C<sub>6</sub>H<sub>6</sub>O<sub>2</sub>), 4-Chlorocatechol (4-CC, C<sub>6</sub>H<sub>5</sub>ClO<sub>2</sub>), benzoquinone (BQ, C<sub>6</sub>H<sub>4</sub>O<sub>2</sub>), hydroxyhydroquinone (HHQ, C<sub>6</sub>H<sub>6</sub>O<sub>2</sub>), and 5-Chloro-1,2,4-benzenetriol (C<sub>6</sub>H<sub>5</sub>ClO<sub>3</sub>) [6, 57, 58]. In the first step 4-chlorophenol is oxidized to 4-CC<sub>(II)</sub> and HQ<sub>(III)</sub>; Then 4-CC is further oxidized 5-Chloro-1,2,4-benzenetriol<sub>(IV)</sub> and HHQ<sub>(V)</sub>. Meanwhile, HQ is changed to HHQ and into BQ<sub>(VI)</sub>. On further oxidation, the benzene rings are opened to form the carboxylic acids, including maleic acid<sub>(VII)</sub> (C<sub>4</sub>H<sub>4</sub>O), formic acid<sub>(VIII)</sub> (CH<sub>2</sub>O<sub>2</sub>), oxalic acid<sub>(IX)</sub> (C<sub>2</sub>H<sub>2</sub>O<sub>4</sub>), acetic acid<sub>(X)</sub> (C<sub>2</sub>H<sub>4</sub>O<sub>2</sub>), and acrylic acid<sub>(XI)</sub> (C<sub>3</sub>H<sub>4</sub>O<sub>2</sub>). Finally, after a few steps of carboxylic acids oxidation, complete mineralization to CO<sub>2</sub> + H<sub>2</sub>O was resulted.

**Kinetic study**

The Langmuir–Hinshelwood (L–H) model is commonly employed to evaluate the degradation reactions kinetics of phenolic compounds by photocatalysts in aqueous medium [59, 60]. The relationship between the degradation rate (r) and the 4-CP concentration (C) is stated by the kinetic model, as:

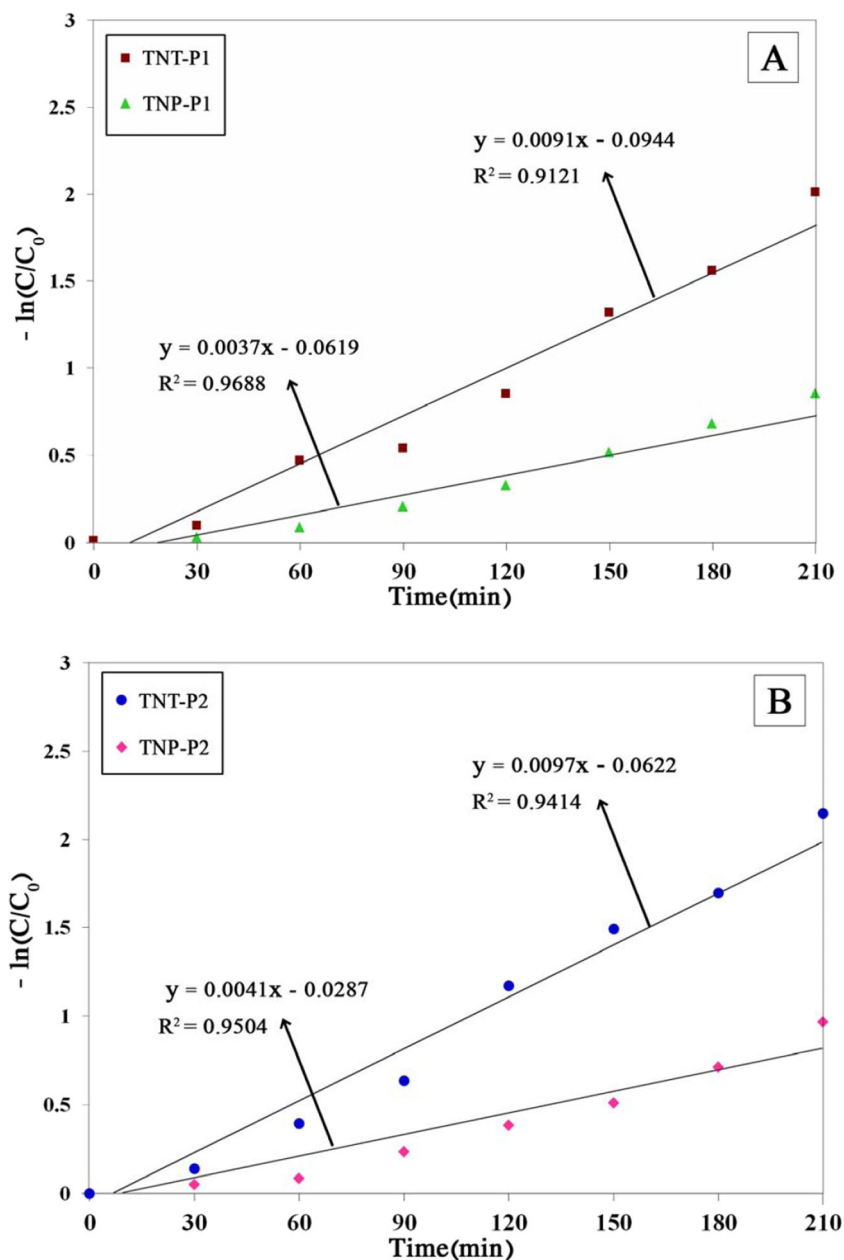
$$r = -\frac{dC}{dt} = \frac{(k_r K_{ad} C)}{(1 + K_{ad} C)} \tag{10}$$

When, k<sub>r</sub> is the inherent rate coefficient (M/min), t is the time of irradiation (min), and K<sub>ad</sub> is the adsorption equilibrium constant of 4-CP on the surface of the photocatalyst (M<sup>-1</sup>), whereas it is rightly tentative that the principal of degradation mechanism is not adsorption, Eq. (10) is simplified to Eq. (11):

$$\ln\left(\frac{C}{C_0}\right) = -k_r K_{ad} t = -k_{app} t \tag{11}$$

When pseudo-first-order kinetic is valid, the diagram of -ln(C/C<sub>0</sub>) vs. t must obtain a linear relation, as expressed in Eq.

**Fig. 14** Kinetic studies for photocatalytic degradation of 4-CP by TiO<sub>2</sub> nanostructures under UV irradiation, catalyst loading: 2 g/L, pH: 4 and 4-CP concentration: 50 mg/L.



(11). Consequently,  $K_{app}$  is estimated from the slope of the diagram. Figure 14(a and b) presents that the pseudo-first-order model acceptably matches with the obtained experimental results.

## Conclusions

In the present study, TiO<sub>2</sub> nanostructures from different titania precursors were obtained via a hydrothermal method in a two-step procedure. The physicochemical, optical, and morphological characteristics of the obtained TiO<sub>2</sub> samples were characterized using advanced analysis techniques. According to

the characterization tests, TNP-P1 and TNP-P2 were prepared with a crystallite size of 17 nm and 7 nm and a surface area 46.24 and 61.31  $\frac{m^2}{g}$ , respectively. Next, TNT-P1 and TNT-P2 were synthesized with a great improvement in surface area (138.83, 167.57  $\frac{m^2}{g}$ ).

The photocatalytic activity of nanostructures was tested for degradation of 4-CP. The results revealed that 1D TNTs showed an improvement in photocatalytic performance compared with the TNPs, demonstrating the benefits of TNTs as photocatalysts for water purification. Moreover, TiO<sub>2</sub> nanostructures prepared from the TALH precursor had higher photocatalytic degradation efficiency than the TTIP precursor. This phenomenon may be ascribed to the fact that TALH is

more stable with regard to hydrolysis than the common alkoxides, as the chelating lactate group and the Ti ion tend to possess an octahedral coordination in this compound, which also accounts for its higher stability compared to titanium alkoxides.

**Acknowledgements** This work was supported by the Petroleum University of Technology (PUT), Abadan Faculty of Petroleum University, Abadan, Iran. The authors thank the PUT for the financial support.

**Authors' contributions** MF conceived the project. AP wrote the initial drafts of the work. AP designed the experiments, synthesized and characterized the materials. AP, MF, and BR analyzed the data. All authors discussed the results of the manuscript. All authors read and approved the final manuscript.

**Funding** This research has been supported financially by Petroleum University of Technology (PUT), Abadan Faculty of Petroleum University, Abadan, Iran.

## Compliance with ethical standards

**Competing interests** The authors declare that they have no competing interests.

**Consent for publication** “Not applicable”.

**Ethics approval and consent to participate** “Not applicable”.

## References

- Zhang W, Wang C-B, Lien H-L. Treatment of chlorinated organic contaminants with nanoscale bimetallic particles. *Catal Today*. 1998;40:387–95.
- Nguyen AT, Juang R-S. Photocatalytic degradation of p-chlorophenol by hybrid H<sub>2</sub>O<sub>2</sub> and TiO<sub>2</sub> in aqueous suspensions under UV irradiation. *J Environ Manag*. 2015;147:271–7.
- Mahmiani Y, Sevim AM, Gül A. Photocatalytic degradation of 4-chlorophenol under visible light by using TiO<sub>2</sub> catalysts impregnated with co(II) and Zn(II) phthalocyanine derivatives. *J Photochem Photobiol A Chem*. 2016;321:24–32.
- Hashemzadeh F, Gaffarinejad A, Rahimi R. Porous p-NiO/n-Nb<sub>2</sub>O<sub>5</sub> nanocomposites prepared by an EISA route with enhanced photocatalytic activity in simultaneous Cr (VI) reduction and methyl orange decolorization under visible light irradiation. *J Hazard Mater*. 2015;286:64–74.
- Mazloomi Tabaei HS, Kazemeini M, Fattahi M. Preparation and characterization of visible light sensitive nano titanium dioxide photocatalyst. *Sci Iran*. 2012;19:1626–31.
- Thomas J, Radhika S, Yoon M. Nd<sup>3+</sup> doped TiO<sub>2</sub> nanoparticles incorporated with heteropoly phosphotungstic acid: a novel solar photocatalyst for degradation of 4-chlorophenol in water. *J Mol Catal A Chem*. 2016;411:146–56.
- Li F, Dai Y, Gong M, Yu T, Chen X. Synthesis, characterization of magnetic-sepiolite supported with TiO<sub>2</sub>, and the photocatalytic performance over Cr (VI) and 2, 4-dichlorophenol co-existed wastewater. *J Alloys Compd*. 2015;638:435–42.
- Barros WRP, Ereno T, Tavares AC, Lanza MRV. In situ electrochemical generation of hydrogen peroxide in alkaline aqueous solution by using an unmodified gas diffusion electrode. *ChemElectroChem*. 2015;2:714–9.
- Yan L, Huang Y, Cui J, Jing C. Simultaneous as(III) and cd removal from copper smelting wastewater using granular TiO<sub>2</sub> columns. *Water Res*. 2015;68:572–9.
- Wang JC, Ren J, Yao HC, Zhang L, Wang JS, Zang SQ, et al. Synergistic photocatalysis of Cr(VI) reduction and 4-Chlorophenol degradation over hydroxylated Fe<sub>2</sub>O<sub>3</sub> under visible light irradiation. *J Hazard Mater*. 2016;311:11–9.
- Wang M, Fang G, Liu P, Zhou D, Ma C, Zhang D, et al. Fe<sub>3</sub>O<sub>4</sub>@β-CD nanocomposite as heterogeneous Fenton-like catalyst for enhanced degradation of 4-chlorophenol (4-CP). *Appl Catal B Environ*. 2016;188:113–22.
- Wang Q, Jiang H, Zang S, Li J, Wang Q. Gd, C, N and P quaternary doped anatase-TiO<sub>2</sub> nano-photocatalyst for enhanced photocatalytic degradation of 4-chlorophenol under simulated sunlight irradiation. *J Alloys Compd*. 2014;586:411–9.
- Li S, Xu Y, Wang X, Guo Y, Mu Q. Catalytic degradation of 4-chlorophenol with La/TiO<sub>2</sub> in a dielectric barrier discharge system. *RSC Adv*. 2016;6:28994–9002.
- Zhu Z, Liu F, Zhang H, Zhang J, Han L. Photocatalytic degradation of 4-chlorophenol over ag/MFe<sub>2</sub>O<sub>4</sub> (M = co, Zn, cu, and Ni) prepared by a modified chemical co-precipitation method: a comparative study. *RSC Adv*. 2015;5:55499–512.
- Pozan GS, Kambur A. Significant enhancement of photocatalytic activity over bifunctional ZnO–TiO<sub>2</sub> catalysts for 4-chlorophenol degradation. *Chemosphere*. 2014;105:152–9.
- Zouzelka R, Kusumawati Y, Remzova M, Rathousky J, Pauporté T. Photocatalytic activity of porous multiwalled carbon nanotube-TiO<sub>2</sub> composite layers for pollutant degradation. *J Hazard Mater*. 2016;317:52–9.
- Zhai Q, Zhang L, Zhao X, Chen H, Yin D, Li J, et al. A novel iron-containing polyoxometalate heterogeneous photocatalyst for efficient 4-chlorophenol degradation by H<sub>2</sub>O<sub>2</sub> at neutral pH. *Appl Surf Sci*. 2016;377:17–22.
- Naeem K, Ouyang F. Influence of supports on photocatalytic degradation of phenol and 4-chlorophenol in aqueous suspensions of titanium dioxide. *J Environ Sci*. 2013;25:399–404.
- Di J, Chen J, Ji M, Zhang Q, Xu L, Xia J. Reactable ionic liquid induced homogeneous carbon superdoping of BiPO<sub>4</sub> for superior photocatalytic removal of 4-chlorophenol. *Chem Eng J*. 2016;313:1477–85.
- Wong CL, Tan YN, Mohamed AR. A review on the formation of titania nanotube photocatalysts by hydrothermal treatment. *J Environ Manag*. 2011;92:1669–80.
- Chen X, Mao SS. Titanium dioxide nanomaterials: synthesis, properties, modifications, and applications. *Chem Rev*. 2007;107:2891–959.
- Liu N, Chen X, Zhang J, Schwank JW. A review on TiO<sub>2</sub>-based nanotubes synthesized via hydrothermal method: formation mechanism, structure modification, and photocatalytic applications. *Catal Today*. 2014;225:34–51.
- Zhang Y, Jiang Z, Huang J, Lim LY, Li W, Deng J. Titanate and titania nanostructured materials for environmental and energy applications: a review. *RSC Adv*. 2015;5:79479–510.
- Cargnello M, Gordon TR, Murray CB. Solution-phase synthesis of titanium dioxide nanoparticles and nanocrystals. *Chem Rev*. 2014;114:9319–45.
- Miranda-Sánchez J, Elizalde I, Lartundo-Rojas L, Hernández-Pérez I, Jaramillo-Vigueras D, Ramírez-López R. The effect of titania precursors and ceria loadings on textural and chemical properties of TiO<sub>2</sub>–CeO<sub>2</sub> and Pt–Rh/TiO<sub>2</sub>–CeO<sub>2</sub>. *J Sol-Gel Sci Technol*. 2015;74:707–17.
- Behzadnia A, Montazer M, Rashidi A, Rad MM. Sonosynthesis of nano TiO<sub>2</sub> on wool using titanium isopropoxide or butoxide in



- acidic media producing multifunctional fabric. *Ultrason Sonochem.* 2014;21:1815–26.
27. Berki P, Reti B, Terzi K, Bountas I, Horvath E, Fejes D, et al. The effect of titania precursor on the morphology of prepared TiO<sub>2</sub>/MWCNT nanocomposite materials. *Phys Status Solidi.* 2014;251:2384–8.
  28. Chae SY, Park MK, Lee SK, Kim TY, Kim SK, Lee WI. Preparation of size-controlled TiO<sub>2</sub> nanoparticles and derivation of optically transparent photocatalytic films. *Chem Mater.* 2003;15:3326–31.
  29. Tang Z-RR, Li F, Zhang Y, Fu X, Xu Y-JJ. Composites of titanate nanotube and carbon nanotube as photocatalyst with high mineralization ratio for gas-phase degradation of volatile aromatic pollutant. *J Phys Chem C.* 2011;115:7880–6.
  30. Kandiel TA, Feldhoff A, Robben L, Dillert R, Bahnemann DW. Tailored titanium dioxide nanomaterials: anatase nanoparticles and brookite nanorods as highly active photocatalysts. *Chem Mater.* 2010;22:2050–60.
  31. Mohammadzadeh S, Olya ME, Arabi AM, Shariati A, Khosravi Nikou MR. Synthesis, characterization and application of ZnO-ag as a nanophotocatalyst for organic compounds degradation, mechanism and economic study. *J Environ Sci.* 2015;35:194–207.
  32. Xiong L, Yang Y, Mai J, Sun W, Zhang C, Wei D. Adsorption behavior of methylene blue onto titanate nanotubes. *Chem Eng J.* 2010;156:313–20.
  33. Pasandideh EK, Kakavandi B, Nasserli S, Mahvi AH, Nabizadeh R, Esrafil A, et al. Silica-coated magnetite nanoparticles core-shell spheres (Fe<sub>3</sub>O<sub>4</sub>@SiO<sub>2</sub>) for natural organic matter removal. *J Environ Health Sci Eng.* 2016;14:21.
  34. Zeng Y, Wang X, Wang H, Dong Y, Ma Y, Yao J. Multi-shelled titania hollow spheres fabricated by a hard template strategy: enhanced photocatalytic activity. *Chem Commun.* 2010;46:4312–4.
  35. Lin H, Huang C, Li W, Ni C, Shah S, Tseng Y. Size dependency of nanocrystalline TiO<sub>2</sub> on its optical property and photocatalytic reactivity exemplified by 2-chlorophenol. *Appl Catal B Environ.* 2006;68:1–11.
  36. Madhusudan Reddy K, Gopal Reddy CV, Manorama SV. Preparation, characterization, and spectral studies on Nanocrystalline Anatase TiO<sub>2</sub>. *J Solid State Chem.* 2001;158:180–6.
  37. Choudhury B, Bayan S, Choudhury A, Chakraborty P. Narrowing of band gap and effective charge carrier separation in oxygen deficient TiO<sub>2</sub> nanotubes with improved visible light photocatalytic activity. *J Colloid Interface Sci.* 2016;465:1–10.
  38. Liu Z, Zhang Q, Qin L-C. Reduction in the electronic band gap of titanium oxide nanotubes. *Solid State Commun.* 2007;141:168–71.
  39. Liu W, Zhao X, Borthwick AGL, Wang Y, Ni J. Dual-enhanced photocatalytic activity of Fe-deposited titanate nanotubes used for simultaneous removal of as (III) and as (V). *ACS Appl Mater Interfaces.* 2015;7:19726–35.
  40. Xiong L, Chen C, Chen Q, Ni J. Adsorption of Pb (II) and cd (II) from aqueous solutions using titanate nanotubes prepared via hydrothermal method. *J Hazard Mater.* 2011;189:741–8.
  41. El-Sheikh SM, Khedr TM, Zhang G, Voghazi V, Ismail AA, Shea KO. Tailored synthesis of anatase–brookite heterojunction photocatalysts for degradation of cyndrospermopsin under UV–vis light. *Chem Eng J.* 2016;310:428–36.
  42. Ahmadi M, Ramezani H, Jaafarzadeh N, Motlagh HR, Jaafarzadeh N, Mostoufi A, et al. Enhanced photocatalytic degradation of tetracycline and real pharmaceutical wastewater using MWCNT/TiO<sub>2</sub> nano-composite. *J Environ Manag.* 2017;186:55–63.
  43. Hsieh C-TT, Fan W-SS, Chen W-YY, Lin J-YY. Adsorption and visible-light-derived photocatalytic kinetics of organic dye on co-doped titania nanotubes prepared by hydrothermal synthesis. *Sep Purif Technol.* 2009;67:312–8.
  44. Wang N, Li X, Wang Y, Quan X, Chen G. Evaluation of bias potential enhanced photocatalytic degradation of 4-chlorophenol with TiO<sub>2</sub> nanotube fabricated by anodic oxidation method. *Chem Eng J.* 2009;146:30–5.
  45. Fabbri D, Prevot A, Pramauro E. Effect of surfactant microstructures on photocatalytic degradation of phenol and chlorophenols. *Appl Catal B Environ.* 2006;62:21–7.
  46. Shojaie A, Fattahi M, Jorfi S, Ghasemi B. Hydrothermal synthesis of Fe-TiO<sub>2</sub>-ag nano-sphere for photocatalytic degradation of 4-chlorophenol (4-CP): investigating the effect of hydrothermal temperature and time as well as calcination temperature. *J Environ Chem Eng.* 2017;5:4564–72.
  47. Chiou C-H, Wu C-Y, Juang R-S. Photocatalytic degradation of phenol and m-nitrophenol using irradiated TiO<sub>2</sub> in aqueous solutions. *Sep Purif Technol.* 2008;62:559–64.
  48. Jiang T, Zhang L, Ji M, Wang Q, Zhao Q, Fu X. Carbon nanotubes/TiO<sub>2</sub> nanotubes composite photocatalysts for efficient degradation of methyl orange dye. *Particuology.* 2013;11:737–42.
  49. Gholami M, Nassehinia HR, Jonidi-Jafari A, Nasserli S, Esrafil A. Comparison of Benzene & Toluene removal from synthetic polluted air with use of Nano photocatalyticTiO<sub>2</sub>/ZNO process. *J Environ Heal Sci Eng.* 2014;12:45.
  50. Chowdhury P, Moreira J, Goma H, Ray AK. Visible-solar-light-driven photocatalytic degradation of phenol with dye-sensitized TiO<sub>2</sub>: parametric and kinetic study. *Ind Eng Chem Res.* 2012;51:4523–32.
  51. González-Juárez JC, Jiménez-Becerril J, Carrasco-Ábrego H. Influence of pH on the degradation 4-chlorophenol by gamma radiocatalysis using SiO<sub>2</sub>, Al<sub>2</sub>O<sub>3</sub> and TiO<sub>2</sub>. *J Radioanal Nucl Chem.* 2008;275:257–60.
  52. Venkatachalam N, Palanichamy M, Arabindoo B, Murugesan V. Enhanced photocatalytic degradation of 4-chlorophenol by Zr<sup>4+</sup> doped nano TiO<sub>2</sub>. *J Mol Catal A Chem.* 2007;266:158–65.
  53. Kim S, Choi W. Visible-light-induced photocatalytic degradation of 4-chlorophenol and phenolic compounds in aqueous suspension of pure titania: demonstrating the existence of a surface-complex-mediated path. *J Phys Chem B.* 2005;109:5143–9.
  54. Ai Z, Yang P, Lu X. Degradation of 4-chlorophenol by a microwave assisted photocatalysis method. *J Hazard Mater.* 2005;124:147–52.
  55. Poorkarimi A, Karimi-Jashni A, Javadpour S. Optimization of toluene removal over W-doped TiO<sub>2</sub> nano-photocatalyst under visible light irradiation. *Environ Technol.* 2017;1–14. <https://doi.org/10.1080/09593330.2017.1375021>.
  56. Zhao C, Pelaez M, Dionysiou DD, Pillai SC, Byrne JA, O'Shea KE. {UV} and visible light activated TiO<sub>2</sub> photocatalysis of 6-hydroxymethyl uracil, a model compound for the potent cyanotoxin cylindrospermopsin. *Catal Today.* 2014;224:70–6.
  57. Li X, Cabbage JW, Tetzlaff TA, Jenks WS. Photocatalytic degradation of 4-chlorophenol. 1. The hydroquinone pathway. *J Org Chem.* 1999;64:8509–24.
  58. Li X, Cabbage JW, Jenks WS. Photocatalytic degradation of 4-chlorophenol. 2. The 4-chlorocatechol pathway. *J Org Chem.* 1999;64:8525–36.
  59. Payan A, Fattahi M, Jorfi S, Roozbehani B, Payan S. Synthesis and characterization of titanate nanotube/single-walled carbon nanotube (TNT/SWCNT) porous nanocomposite and its photocatalytic activity on 4-Chlorophenol degradation under UV and solar irradiation. *Appl Surf Sci.* 2018;434:336–50.
  60. Alimoradzadeh R, Assadi A, Nasserli S, Mehrasbi MR. Photocatalytic degradation of 4-chlorophenol by UV/H<sub>2</sub>O<sub>2</sub>/NiO process in aqueous solution. *J Environ Health Sci Eng.* 2012;9:12.